THE JOURNAL OF PHYSICAL CHEMISTRY C

ARTICLE

pubs.acs.org/JPCC

Theoretical Characterization of the $PC_{60}BM$:PDDTT Model for an Organic Solar Cell

Yuanzuo Li,[†,‡] Tonu Pullerits,[§] Meiyu Zhao,[∥,⊥] and Mengtao Sun*[,†]

[†]Beijing National Laboratory for Condensed Matter Physics, Institute of Physics, Chinese Academy of Sciences, P.O. Box 603-146, Beijing, 100190, People's Republic of China

[‡]College of Science, Northeast Forestry University, Harbin 150040, People's Republic of China

[§]Department of Chemical Physics, Lund University, Box 124, Lund 22100, Sweden

[∥]Institute of Theoretical Simulation Chemistry, Academy of Fundamental and Interdisciplinary Sciences, Harbin Institute of Technology, Harbin 150080, People's Republic of China

[⊥]Department of Chemistry, University of Alberta, Edmonton, Alberta T6G 2G2, Canada

ABSTRACT: We use time-dependent density functional theory together with a set of extensive multidimensional visualization techniques to characterize band gap, optical absorption properties, intramolecular and intermolecular charge transfer, exciton binding energy, charge transfer integral, and the rate of charge transfer and recombination in the $PC_{60}BM$:PDDTT model of an organic solar cell. These theoretical methods and calculation techniques not only promote deeper understanding of the connection between chemical structures and the optical and electronic properties of the donor−acceptor system but also can be used to rational design novel donor−acceptor system.

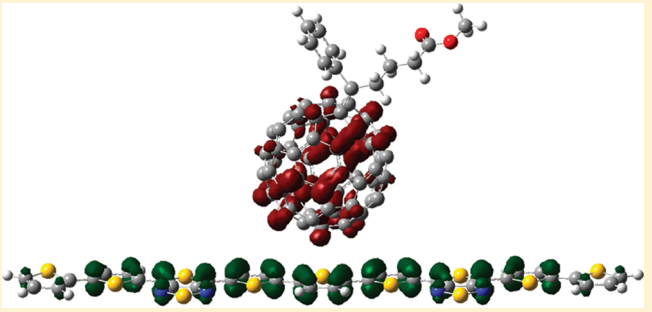

1. INTRODUCTION

The annual energy input of solar irradiation on Earth (5% UV, 43% visible, 52% IR) exceeds the world's yearly energy consumption by several orders of magnitude.[1] In this context organic solar cells are becoming very attractive, due to their numerous potential advantages over traditional silicon-based solar cells. For example low cost, flexibility, large-area capability, and easy processing.[2] The active layers in organic solar cells typically consist of two components, an electron donor (D) and an electron acceptor (A) material, assembled either into a bilayer structure or in the form of a blend.[3] Fullerene and its derivates are the most used electron-acceptor materials.[4−6] For the electron donor materials, one of the most important properties is a strong absorption covering a broad spectral region whereas the band gap is less than 2 eV.[7−10] Another important issue is minimizing the loss processes in the bulk during the exciton and charge transport. The photocurrent generation in the polymer solar cells generally involves five steps:[5] (1) absorption of light by the active layer, resulting in creation of excitons; (2) excitons transport to the donor−acceptor interface; (3) dissociation of excitons at the interface of electron donor/acceptor and formation of free charges; (4) transport of the charges under an electric field; and (5) charge collection by electrodes.

In order to promote deeper understanding of the connection between chemical structures and the optical and electronic properties of the donor−acceptor system, and rational design of novel donor−acceptor systems, theoretical calculations play an important role. From the viewpoint of electronic structure, the donor−acceptor system should have strong electronic coupling whereas the exciton binding energy should be low. Quantum mechanical calculations on donor−acceptor complexes can provide important information about these properties and predict optical absorption spectra of the donor−acceptor system.[3] In order to be manageable, in these calculations the complex issues of a realistic condensed phase environment of the donor−acceptor system are usually neglected. In order to evaluate such calculations, some key results have to be compared with experiment. The exciton binding energy is easy to check with an optical experiment. An electrochemistry experiment can be used to evaluate the oxidation and reduction potentials, which reveal the HOMO−LUMO gap.[11] Femtosecond transient absorption and time-resolved emission measurements can be employed to study the dynamics of charge transfer and charge recombination.[11] Time-resolved studies of the solar cells are of particular importance since the transport of the charges in a cell is under the influence of an external electric field.[12] Marcus theory[13] has been widely employed to describe the dynamics of charge transfer and charge recombination in any donor−acceptor system including the organic solar cells. To obtain efficient charge transfer and slow charge recombination, the ΔG (the free energy change) should be optimized.[14]

Recently, Gong et al.[9] experimentally investigated highly efficient polymer photodetectors (PDs) with broad spectral response from

Received: May 15, 2011
Revised: September 8, 2011
Published: September 27, 2011

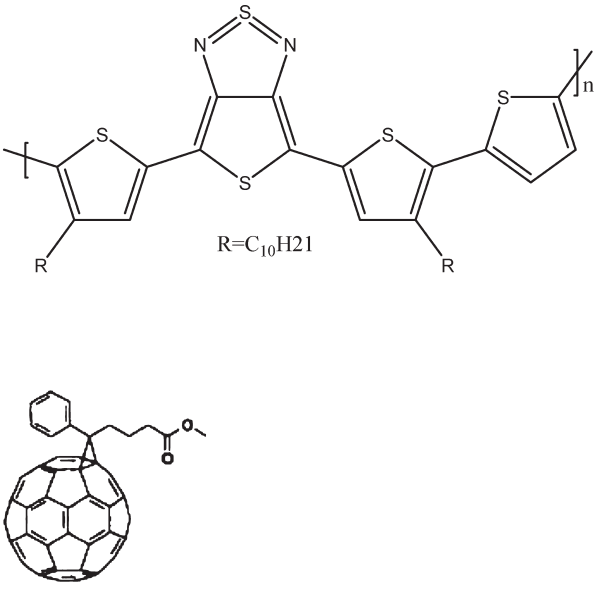

Figure 1. Chemical structures of PDDTT and $PC_{60}BM$.

300 to 1450 nm. The devices are composed of a narrow band gap poly(5,7-bis(4-decanyl-2-thienyl)-thieno(3,4-*b*)diathiazole-thiophene-2,5) (PDDTT) and (6,6)-phenyl-C_{61}-butyric acid methyl ester ($PC_{60}BM$), and the efficiency of the polymer PD is comparable to or even better than those from Si and InGaAs PDs. Stimulated by this recent experimental report, we investigate the electronic structure, electronic coupling, and optical properties of the system using quantum chemistry. Directionality and electron−hole coherence of charge transfer upon electronic transitions are investigated with the three-dimensional (3D) real space representation[15] and the two-dimensional (2D) site representation.[16] We also calculate dynamics of charge transfer and charge recombination using Marcus theory. We conclude that the system is an excellent candidate for donor−acceptor heterojunction for organic solar cell.

2. METHODS

All quantum chemistry calculations were done with Gaussian 09 software.[17] The ground-state geometries of $PC_{60}BM$, PDDTT (see Figure 1), and $PC_{60}BM$−PDDTT complex were optimized with density functional theory (DFT),[18] B3LYP functional,[19] and 6-31G(d) basis set. In the calculations, R = $C_{10}H_{21}$ (the side chain of PDDTT) was repacked by H, because they merely aid in improving solubility without affecting electronic properties.[20] In the calculations of PDDTT and $PC_{60}BM$−PDDTT complex, n = 1 and 2 are used to study the size effect on optical absorption. When n = 2, an additional thiophene was added to keep the symmetry. Partial density of states (PDOS) were visualized with GaussSum software.[21] To study the reorganization energy in Marcus theory, the positively charged geometry of PDDTT and negatively charged geometry of $PC_{60}BM$ were also optimized with DFT, B3LYP functional, 6-31G(d) basis set, and then the energy of the neutral $PC_{60}BM$, based on the optimized negative charged geometry, was obtained from single point energy calculations at the same level of theory. Electronic transitions in optical absorption were computed with time-dependent DFT (TD-DFT),[22] CAM-B3LYP functional,[23] and 6-31G(d) basis set. Note that the long-range-corrected functional (CAM-B3LYP)[23] was employed for the non-Coulomb part of exchange functional. Tretiak et al.[24] have studied exciton size in conducting polymers by TD-DFT, using the adiabatic local density approximation (ALDA), gradient-corrected functionals, and hybrid functionals, and found that B3LYP represents a practical and accurate way for the correct description of excited states in such systems. They found that the B3LYP results are in good agreement with experimental band gap. To calculate charge transfer integral (electronic coupling matrix), the Generalized Mulliken−Hush (GMH) model[25] and the finite field method on the excitation energy of the donor−acceptor heterojunction were employed.[26]

The TD-DFT calculations provide the singlet excited states $|S_n\rangle$ represented by vectors $C^{CI}_{n,ai}$ based on configurations of unoccupied and occupied molecular orbitals a and i, respectively. The molecular orbitals are in turn given by linear combination of atomic orbitals (LCAO) μ and ν with coefficients $c^{LCAO}_{a\mu}$ and $c^{LCAO}_{a\nu}$. In order to characterize the excited stat,e we define two matrixes[15]

$$Q^{(n)}_{\mu\nu} = \frac{1}{\sqrt{2}} \sum_{\substack{a \in unocc \\ i \in occ}} C^{CI}_{n,ai}\left(c^{LCAO}_{a\mu}c^{LCAO}_{i\nu} + c^{LCAO}_{i\mu}c^{LCAO}_{a\nu}\right)$$

$$P^{(n)}_{\mu\nu} = \frac{i}{\sqrt{2}} \sum_{\substack{a \in unocc \\ i \in occ}} C^{CI}_{n,ai}\left(c^{LCAO}_{a\mu}c^{LCAO}_{i\nu} - c^{LCAO}_{i\mu}c^{LCAO}_{a\nu}\right) \quad (1)$$

which are (anti)symmetric for exchange of the atomic orbitals and normalized as

$$\sum_{\mu,\nu} |Q^{(n)}_{\mu\nu}|^2 = \sum_{\mu,\nu} |P^{(n)}_{\mu\nu}|^2 = 1 \quad (2)$$

In the collective electron oscillator (CEO) model[16] the excited state $|S_n\rangle$ is described by a harmonic oscillator with oscillating coordinate $Q^{(n)}_{\mu\nu}\cos(\omega_n t)$ and momentum $P^{(n)}\sin(\omega_n t)$ for the transition frequency ω_n. For visual characterization of the excited states, we use two different representations of the matrices $Q^{(n)}_{\mu\nu}$ and $P^{(n)}_{\mu\nu}$.

Real-Space Representation. In real space the oscillating CEO coordinate and momentum are given as[15]

$$\begin{aligned} Q_n(\mathbf{r},\mathbf{r}';t) &= \sum_{\mu\nu} \phi^{AO}_\mu(\mathbf{r}) Q^{(n)}_{\mu\nu} \phi^{AO}_\nu(\mathbf{r}') \cos(\omega_n t) \\ P_n(\mathbf{r},\mathbf{r}';t) &= \sum_{\mu\nu} \phi^{AO}_\mu(\mathbf{r}) P^{(n)}_{\mu\nu} \phi^{AO}_\nu(\mathbf{r}') \sin(\omega_n t) \end{aligned} \quad (3)$$

The diagonal slice for $\mathbf{r} = \mathbf{r}'$ results in

$$\begin{aligned} Q_n(\mathbf{r},\mathbf{r};t) &= \sqrt{2}\rho_{n0}(\mathbf{r})\cos(\omega t) \\ P_n(\mathbf{r},\mathbf{r};t) &= 0 \end{aligned} \quad (4)$$

The amplitude of the former is given by the so-called transition density (TD)

$$\rho_{n0}(\mathbf{r}) = \frac{1}{\sqrt{2}} \sum_{\mu,\nu} \phi^{AO}_\mu(\mathbf{r}) Q^{(n)}_{\mu\nu} \phi^{AO}_\nu(\mathbf{r}) \quad (5)$$

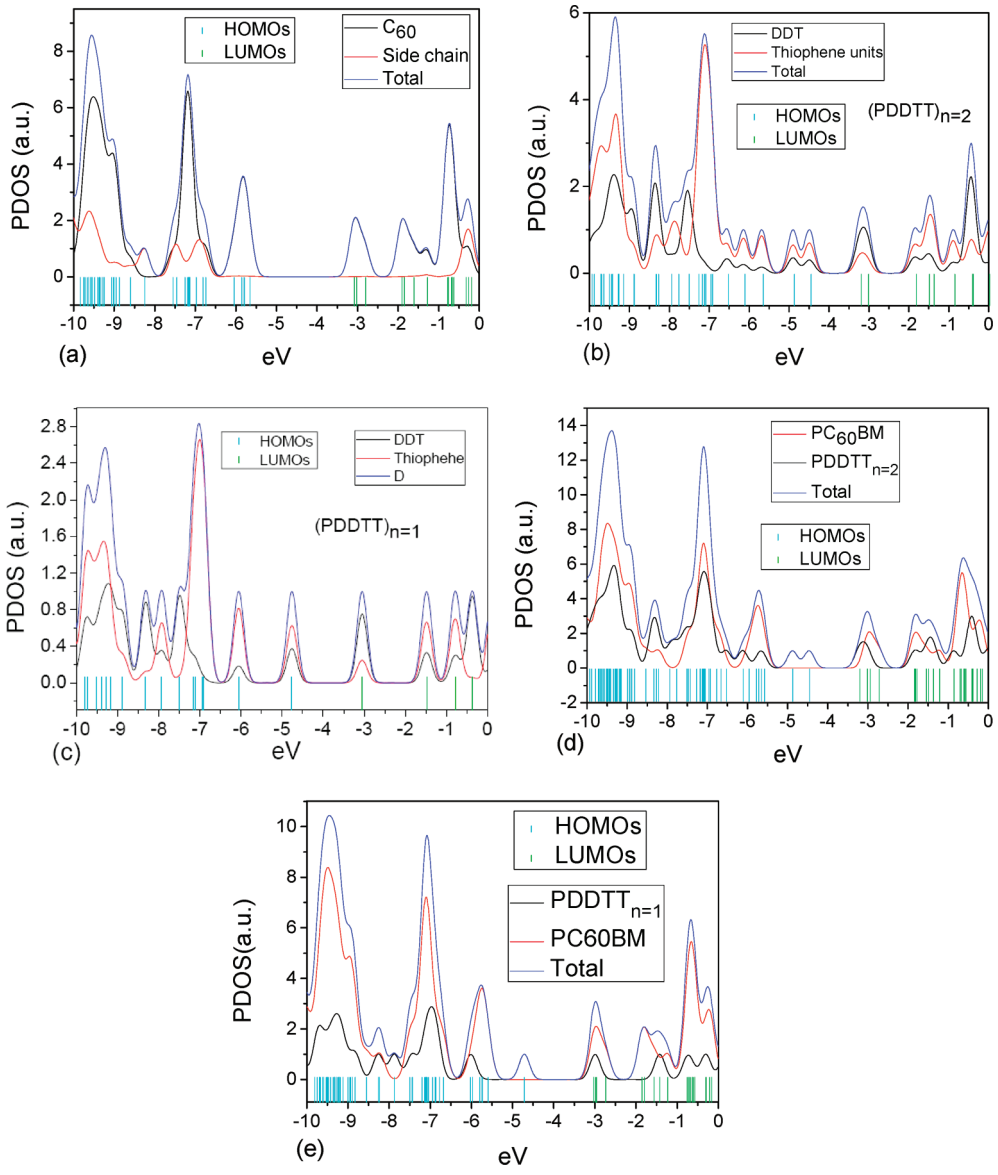

Figure 2. Partial density of state (PDOS) of $PC_{60}BM$, PDDTT with $n = 2$ and 1, $PC_{60}BM-PDDTT_{n=2}$ and $PC_{60}BM-PDDTT_{n=1}$.

The transition density contains information about the spatial location of the excitation[27] and is directly related to the transition dipole

$$\boldsymbol{\mu}_{n0} = e \int r\rho_{n0}(r)\, \mathrm{d}^3 r \tag{6}$$

Besides the transition density, the charge difference density (CDD)[28]

$$\Delta\rho_{nn}(\mathbf{r}) = 2i \sum_{\mu,\nu,\kappa} \phi_{\mu}^{\mathrm{AO}}(\mathbf{r}) Q_{\kappa\mu}^{(n)} P_{\kappa\nu}^{(n)} \phi_{\nu}^{\mathrm{AO}}(\mathbf{r}) \tag{7}$$

is an important quantity for real-space characterization of excitons. It represents the difference of electron distribution between the excited state $|S_n\rangle$ and the ground state $|S_0\rangle$. In the present work, both transition and charge difference density are represented by isosurfaces based on a 3D grid of approximately 100000 cubes.

Site Representation. For site representation of the CEO coordinate and momentum we define

$$\overline{Q_{\mathrm{AB}}^{(n)2}} = \sum_{\substack{\mu \in \mathrm{A} \\ \nu \in \mathrm{B}}} |Q_{\mu\nu}^{(n)}|^2 \quad \text{and} \quad \overline{P_{\mathrm{AB}}^{(n)2}} = \sum_{\substack{\mu \in \mathrm{A} \\ \nu \in \mathrm{B}}} |P_{\mu\nu}^{(n)}|^2 \tag{8}$$

respectively.[15,29] This means that the matrices $Q_{\mu\nu}^{(n)}$ and $P_{\mu\nu}^{(n)}$ are merged for atomic orbitals belonging to atomic sites A and B, respectively. Thus $\overline{P_{\mathrm{AB}}^{(n)2}}$ gives the intensity of electron−hole oscillations between the atomic sites A and B in electronic state n, while $\overline{Q_{\mathrm{AB}}^{(n)2}}$ is a measure of the delocalization of the exciton. Note that for Frenkel excitons the occupation of $\overline{Q_{\mathrm{AB}}^{(n)2}}$ and $\overline{P_{\mathrm{AB}}^{(n)2}}$ is limited to pairs of atomic centers A and B belonging to the same monomeric unit. For the neutral polymer, only $\overline{Q_{\mathrm{AB}}^{(n)2}}$ is employed, since the excited state properties of $\overline{P_{\mathrm{AB}}^{(n)2}}$ are similar to $\overline{Q_{\mathrm{AB}}^{(n)2}}$. For the charged polymer both $\overline{P_{\mathrm{AB}}^{(n)2}}$ and $\overline{Q_{\mathrm{AB}}^{(n)2}}$ need to be used.[15] Analogous the real-space wave function mapping of

dx.doi.org/10.1021/jp2040696 |J. Phys. Chem. C 2011, 115, 21865–21873

Table 1. Calculated Transition Energies (eV, nm) and Oscillator Strengths (f) for Polymer

	$n = 2$			$n = 1$	
	eV (nm)	f	CI coefficients	eV (nm)	f
S_1	1.4551 (852.09)	2.0205	0.61 (H → L)	1.7948 (690.79)	0.4807
S_2	1.7076 (726.06)	0.0001	0.56 (H → L + 1)	3.3548 (369.58)	0.3236
S_3	2.4776 (500.42)	0.0035	0.52 (H − 1 > L)	3.4615 (358.18)	0.4456
S_4	2.6029 (476.34)	0.2937	0.51 (H − 1 > L + 1)		
S_5	2.9778 (416.36)	1.1416	0.57 (H → L + 2)		

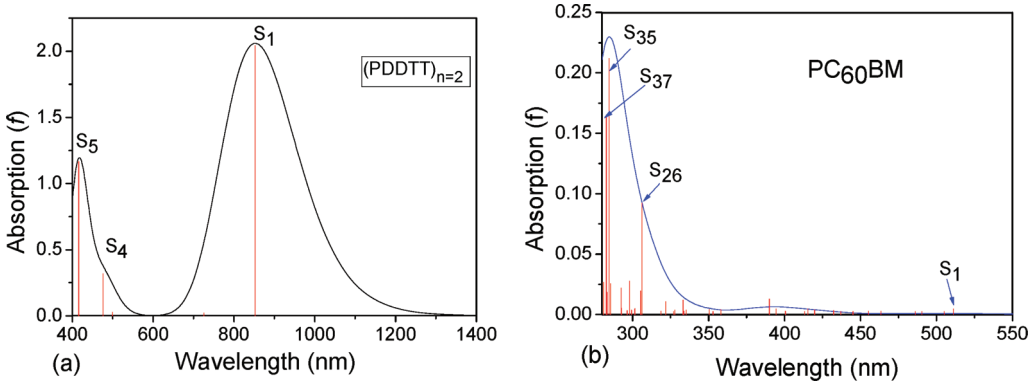

Figure 3. Optical absorption spectra of PDDTT and $PC_{60}BM$.

exciton wave functions have also been computed by Barford and co-workers.[30]

3. RESULTS AND DISCUSSION

3.1. Ground-State Properties. On the basis of the optimized ground-state geometries of $PC_{60}BM$, PDDTT, and $PC_{60}BM$–PDDTT complex, the partial density of states (PDOS) were calculated and are presented in Figure 2. With the PDOS, we can find the % contribution of a group to each molecular orbital. We found that for $PC_{60}BM$ all the density on the C_{60} for HOMOs and LUMOs is in the range from −6.5 to −1 eV, and the band gap ($E_{bg} = |E_{LUMO} - E_{HOMO}|$) is 2.338 eV. Compared with $PC_{60}BM$, the energy level of HOMO of PDDTT is significantly increased (see panels b and c of Figure 2 for $n = 2$ and $n = 1$, respectively), so the open circuit-voltage V_{oc} can be estimated with

$$V_{oc} \leq |E_{HOMO}(D) - E_{LUMO}(A)|/e - 0.3\,V \quad (9)$$

where the value of 0.3 V in eq 9 is an empirical factor.[10] $V_{oc} \approx$ 1.09 V for the unit $n = 2$. Furthermore, from panels b and c of Figure 2, the most density on HOMOs in the range from −7.5 to −4 eV is localized on the thiophene units, while most density on LUMOs around −3 eV is localized on the DDT units, so the electronic transitions involving these orbitals are intramolecular charge transfer excited states, where electron transfer from thiophene to DDT occurs. The band gaps of PDDTT are 1.25 and 1.71 eV for $n = 2$ and $n = 1$, respectively. Therefore, the V_{oc} and E_{bg} will be decreased slightly with the increase of the repeat units of polymer.

From panels d and e of Figure 2, the densities on HOMO and HOMO-1 are fully localized on $PDDTT_{n=2}$, and the energy levels of HOMO and HOMO-1 are similar with that of $PDDTT_{n=1}$. The densities of LUMOs with energy levels below −1.5 eV are almost localized on $PC_{60}BM$, except for that of HOMO, where the density is localized on $PDDTT_{n=2}$. The band gap (E_{bg}) of $PC_{60}BM$-$PDDTT_{n=2}$ complex is E_{bg} = 1.251 eV. For $PC_{60}BM$–$PDDTT_{n=1}$ complex, the E_{bg} = 1.687 eV.

3.2. Electronic Transitions in Optical Absorption. The electronic transitions in optical absorption were calculated with TD-DFT method, where the long-range-corrected functional (CAM-B3LYP)[22] has been employed for the non-Coulomb part of the exchange functional. The calculated transition energies and oscillator strengths of PDDTT are listed in Table 1. It is found that with the increase of units of PDDTT, the first strong peak in absorption is red-shifted by 0.34 eV. The simulated optical absorption spectra of PDDTT can be seen in Figure 3a. There are three strong absorption peaks. Clearly $n = 2$ is already sufficient for PDDTT to perform representative calculations, since the calculated first absorption peak is at 852 nm, and the experimental absorption peak is at 860 nm.

Intramolecular charge transfer upon electronic transitions for PDDTT is visualized with charge difference density. It is found that charge transfer occurs from thiophene units to DDT units in the lowest electronic transition (see Figure 4). The charge transfer properties of S_4 are similar with those of S_1. While for the third strong absorption (S_5), we can see that electron transfers from the outer thiophene unit to the inner thiophene units. These excited state properties were further confirmed by 2D site representation (see Figure 5), where electron–hole coherences are visualized. For S_1, electron–hole coherence is strong between left DDT and the left outer T_2 and inner T_3 but is negligible with the right outer T_2. The same result of electron–hole coherence for right DDT with right outer T_2 and inner T_3 can be seen in Figure 5a. The S_5 is clearly the $\pi\pi^*$ transition on inner T_3, since electron and hole are all localized on that unit (see Figure 5b).

From transition density in Figure 6, one can understand why the S_2 has a weak absorption. There are two subtransition dipole moments with opposite orientations which almost cancel out each other; consequently, the total transition dipole moment is small. For S_1, one can see that the transition dipole moment is a sum of many small transition dipole moments, one per monomeric unit.[15]

The simulated optical absorption spectra of $PC_{60}BM$ can be seen in Figure 3b. We found that the strong absorption peaks (S_{26}, S_{35}, and S_{37}) are within the ultraviolet region. The first singlet excited state is at about 511 nm with a weak absorption. Charge difference density (see Figure 7) reveals that S_1 is localized excitation on C_{60}, since electron and hole are all localized on C_{60}. S_{26}, S_{35}, and S_{37} are dominantly localized excited states (where electron and hole are localized on C_{60}), as well as electrons transfer from phenyl to C_{60}. The calculated electronic transitions with oscillator strengths for the lowest 40 singlet excited states are listed in the Table 2.

Electronic transitions of PDDTT−$PC_{60}BM$ complex are listed in the Table 3. There are three strong absorption peaks S_1, S_{10}, and S_{18}. From charge difference density in Figure 8, we conclude that these three peaks are localized excitations of PDDTT. Electrons transfer from outer and inner thiophene units to DTT units for S_1 and S_{10}, which are similar with those of S_1 and S_4 of PDDTT in Figure 4. For S_{18}, electrons transfer from outer thiophene units to DTT units, and for inner thiophene units, it is a $\pi\pi^*$ transition, which is similar to S_5 of PDDTT in Figure 4. We also conclude from Figure 8 that the lowest intermolecular charge transfer excited state is S_3, and the degenerate excited state S_4 (with S_3) is also an intermolecular charge transfer excited state. Furthermore, S_3 and S_4 are not pure intermolecular charge transfer excited states, since electron and hole are also localized on C_{60}, so for $PC_{60}BM$ it is a localized excited state. S_6 is a pure intermolecular charge transfer excited state, since electron and hole are localized on $PC_{60}BM$ and PDDTT, respectively. S_5 is a pure localized excited state for $PC_{60}BM$—both electron and hole are localized on $PC_{60}BM$.

3.3. Exciton Transport. After formation of excitons, the next step is excitation transport to the donor−acceptor interface. Exciton transport competes with possible loss processes like luminescence or radiative recombination to the ground state. The lifetime of an exciton (τ_{exc}) is determined by the reciprocal value of all radiative and nonradiative decay rates. For an efficient solar cell the majority of excitons should reach the interface within τ_{exc}.

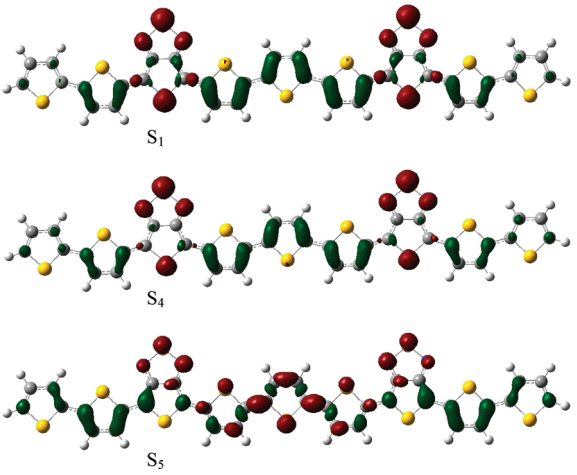

Figure 4. Charge difference densities of the polymer, where the green and red colors stand for the hole and electron, respectively.

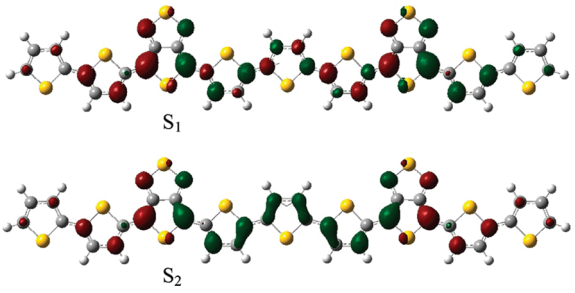

Figure 6. Transition densities of the PDDTT, where the green and red colors stand for the hole and electron, respectively.

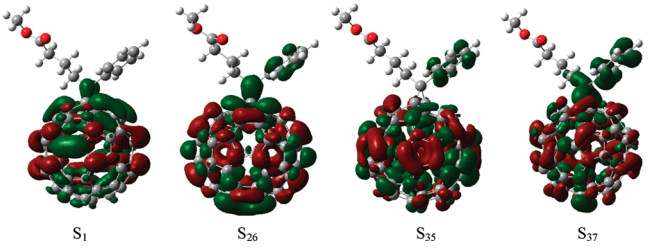

Figure 7. Charge difference densities for different electronic excited states, where the green and red stand for the hole and electron, respectively.

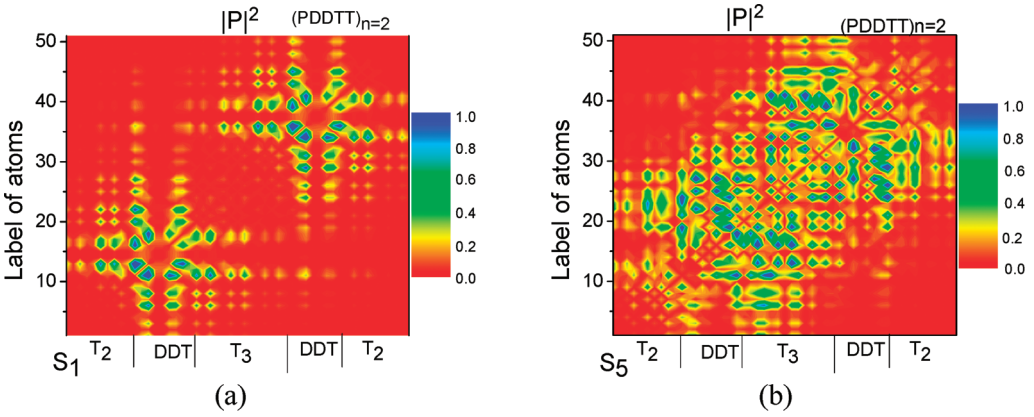

Figure 5. 2D site representation of transition density matrix for S_1 and S_5, and the color bars are shown at the right of figure.

Table 2. Calculated Transition Energies (eV, nm) and Oscillator Strengths (f) for $PC_{60}BM$

	eV (nm)	f
S_1	2.4253 (511.22)	0.0021
S_2	2.4540 (505.23)	0.0000
S_3	2.5277 (490.51)	0.0000
S_4	2.5501 (486.20)	0.0000
S_5	2.6748 (463.52)	0.0001
S_6	2.7224 (455.42)	0.0003
S_7	2.7847 (445.23)	0.0000
S_8	2.8357 (437.23)	0.0000
S_9	2.8672 (432.42)	0.0008
S_{10}	2.9520 (419.99)	0.0013
S_{11}	2.9845 (415.43)	0.0020
S_{12}	3.0005 (413.21)	0.0000
S_{13}	3.0943 (400.69)	0.0001
S_{14}	3.1425 (394.54)	0.0020
S_{15}	3.1784 (390.08)	0.0104
S_{16}	3.4602 (358.32)	0.0015
S_{17}	3.5119 (353.04)	0.0000
S_{18}	3.5376 (350.48)	0.0016
S_{19}	3.6969 (335.37)	0.0012
S_{20}	3.7131 (333.91)	0.0001
S_{21}	3.7189 (333.39)	0.0094
S_{22}	3.7800 (328.00)	0.0011
S_{23}	3.7892 (327.20)	0.0000
S_{24}	3.8513 (321.93)	0.0081
S_{25}	3.8896 (318.76)	0.0001
S_{26}	4.0465 (306.40)	0.0898
S_{27}	4.0585 (305.49)	0.0170
S_{28}	4.1108 (301.61)	0.0023
S_{29}	4.1410 (299.41)	0.0011
S_{30}	4.1585 (298.15)	0.0252
S_{31}	4.1820 (296.47)	0.0007
S_{32}	4.2354 (292.73)	0.0027
S_{33}	4.2377 (292.58)	0.0192
S_{34}	4.3411 (285.60)	0.0232
S_{35}	4.3565 (284.60)	0.2092
S_{36}	4.3753 (283.37)	0.0160
S_{37}	4.3835 (282.84)	0.1617
S_{38}	4.4115 (281.05)	0.0006
S_{39}	4.4136 (280.92)	0.0241
S_{40}	4.4937 (275.91)	0.0467

Transport of the excitons may involve an initial coherent stage followed by incoherent hopping-like diffusion.[31] The distance an exciton is able to cross, L_{exc}, is given by

$$L_{exc} = (D_{exc}\tau_{exc})^{1/2} \quad (10)$$

in which D_{exc} is the diffusion coefficient of the excitons. Usually, τ_{exc} for molecular materials is several nanoseconds, and L_{exc} is generally limited to 10 nm. The dynamics of exciton migration is usually treated with Monte Carlo modeling[32,33] and is beyond the scope of the current study.

3.4. The Exciton Binding Energy. Exciton dissociation is a two-step process,[34] where excitons are first separated to less strongly bound polaron pairs and, finally, to free polarons. In order to dissociate excitons to polarons, the large binding energy has to be overcome. The exciton binding energy is one of the key parameters that govern the physics of many optoelectronic organic devices. It is directly related to the charge separation in organic solar cells. The exciton binding energy mainly originates from the

Table 3. Calculated Transition Energies (eV, nm) and Oscillator Strengths (f) forPDDTT−$PC_{60}BM$

	eV (nm)	f
S_1	1.4558 (851.65)	1.9568
S_2	1.6982 (730.08)	0.0084
S_3	2.4216 (512.00)	0.0009
S_4	2.4288 (510.48)	0.0009
S_5	2.4537 (505.29)	0.0000
S_6	2.4623 (503.54)	0.0000
S_7	2.4795 (500.04)	0.0039
S_8	2.5285 (490.34)	0.0001
S_9	2.5472 (486.74)	0.0000
S_{10}	2.5981 (477.22)	0.2231
S_{11}	2.6391 (469.79)	0.0051
S_{12}	2.6767 (463.20)	0.0001
S_{13}	2.7244 (455.08)	0.0003
S_{14}	2.7867 (444.91)	0.0000
S_{15}	2.8338 (437.52)	0.0000
S_{16}	2.8637 (432.95)	0.0009
S_{17}	2.9523 (419.95)	0.0009
S_{18}	2.9805 (415.99)	1.0130
S_{19}	2.9880 (414.94)	0.0397

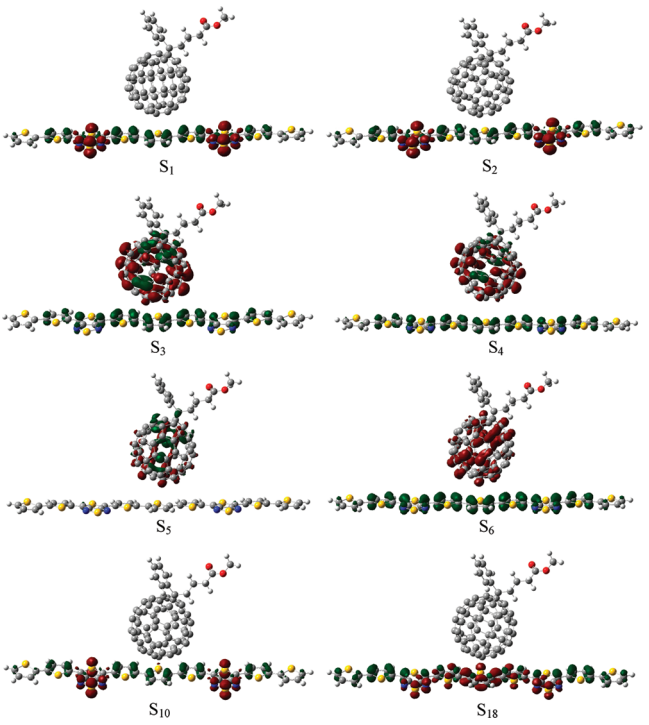

Figure 8. Charge difference densities for different electronic excited states, where the green and red stand for the hole and electron, respectively.

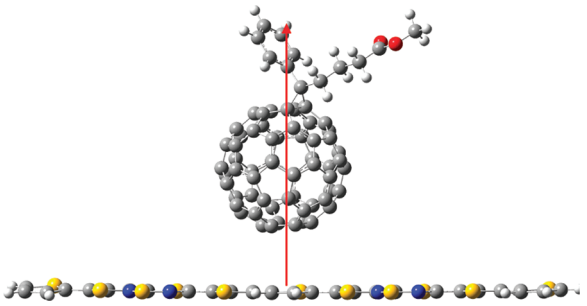

Figure 9. Orientation of the y axis in the complex (perpendicular to PDDTT).

Coulomb interaction energy between the cation of donor and anion of acceptor and is calculated as[35]

$$E_{\mathrm{Coul}} = \sum_{\mathrm{d}\in \mathrm{D},\mathrm{h}\in \mathrm{a}} \varepsilon \frac{q_{\mathrm{d}} q_{\mathrm{a}}}{r_{\mathrm{da}}} \tag{11}$$

where q_{d} and q_{a} are the partial charges on atoms d and a from donor cation and acceptor anion, respectively, r_{da} is the distance between these atoms, and ε is the dielectric constant. The estimation of E_{Coul} from theory can been done using different approaches, which has been discussed before.[15] A charge carrier becomes free from the Coulomb attraction of an opposite charge when $E_{\mathrm{B}} \leq k_{\mathrm{B}}T$, which amounts to 25 meV at room temperature. Usually the exciton binding energy is taken as the difference between the electronic and optical band gap energy.[36] The electronic band gap can be approximated as energy difference of HOMO and LUMO, while the optical gap is taken as the first singlet excitation energy. In that way we obtain the exciton binding energy of PDDTT for $n = 2$ as 0.065 eV.

3.5. Nonlinear Effect on Properties of Electronic Excited States and Photoexcitations. For organic solar cells, the transport of the charges occurs under the influence of an external electric field. Therefore, we will now study properties of excited states and photoexcitations under the external electric field. Linear and nonlinear optical spectroscopies for studying properties of excited states and photoexcitations on organic solar cell have been employed.[12] By use of a finite field method on the excitation energy, the transition energy dependence on the static electric field $\boldsymbol{F}$ can be expressed as[26]

$$E_{\mathrm{exc}}(F) = E_{\mathrm{exc}}(0) - \Delta\mu F - \frac{1}{2}\Delta\alpha F^2 \tag{12}$$

where $E_{\mathrm{exc}}(0) = \Delta E$ is the excitation energy at zero field and $\Delta\alpha$ is the change in the polarizability. We study the nonlinear effect for the third and the forth excited states; since S_3 and S_4 are the lowest intermolecular charge transfer excited states, they are almost degenerate in energy. From the eq 12 we obtain $\Delta\mu = 11.5$ au (29.23 D) and $\Delta\mu = 4.0$ au for S_3 and S_4, respectively. The orientation of external electric field is along the y axis, which can be seen from Figure 9.

3.6. Rate of Charge Transfer in Marcus Theory. The rates of exciton dissociation and charge recombination were evaluated using the Marcus theory[13]

$$k = \sqrt{\frac{4\pi^3}{h^2\lambda k_{\mathrm{B}}T}}|V_{\mathrm{DA}}|^2 \exp\left(-\frac{(\Delta G + \lambda)^2}{4\lambda k_{\mathrm{B}}T}\right) \tag{13}$$

where λ is the reorganization energy, V_{DA} is the electronic coupling (charge-transfer integral) between donor and acceptor, ΔG is the free energy change for the electron transfer reaction, k_{B} is the Boltzmann constant, h is Planck's constant, and T is the temperature (we set $T = 300$ K in our calculations). In the exciton dissociation and charge recombination, $\Delta G = \Delta G_{\mathrm{CT}}$ and ΔG_{CR}, respectively.

The charge transfer integral (electronic coupling matrix) can be calculated with the Generalized Mulliken−Hush (GMH) model.[25] In the two-state (S_0 and S_n states) formulation

$$V_{\mathrm{DA}} = \frac{\mu_{\mathrm{tr}}\Delta E}{\sqrt{(\Delta\mu)^2 + 4(\mu_{\mathrm{tr}})^2}} \tag{14}$$

where μ_{tr} is the calculated transition dipole moment along the y axis (see Figure 9), $\Delta\mu$ is the dipole moment difference between the two states, and ΔE is the vertical excitation energy. $\Delta\mu$ in eq 14 can be estimated by using a finite field method on the excitation energy (see above). Since S_1 and S_2 of PDDTT−PC_{60}BM complex are localized excited states of PDDTT. $V_{\mathrm{DA}}(S_{3\leftarrow 0})$) was estimated with S_3, which is the lowest intermolecular charge transfer excited state, and the calculated $\mu_{\mathrm{tr}} = 0.0312$ au (0.0973 D) for S_3 and the fitted $V_{\mathrm{DA}}(S_{3\leftarrow 0}) \approx 49.0$ cm^{-1}. Note that the S_3 and S_4 charge transfer excited states are degenerate in energy, so we should also consider the three-state Mulliken−Hush model. The calculated $\mu_{\mathrm{tr}} = 0.0079$ au (0.02 D) for S_4 and $V_{\mathrm{DA}}(S_{4\leftarrow 0}) \approx 17.0$ cm^{-1}. So, considering the three-state Mulliken−Hush, $V_{\mathrm{DA}} = V_{\mathrm{DA}}(S_{3\leftarrow 0}) + V_{\mathrm{DA}}(S_{4\leftarrow 0}) = 66.0$ cm^{-1}.

The reorganization energy λ consists of inner reorganization energy and outer reorganization energy.[37] The inner reorganization energy arises from the change in equilibrium geometry of the donor (D) and acceptor (A) sites consecutive to the gain or loss of electronic charge upon electron transfer. The outer reorganization energy is due to the electronic and nuclear polarization/relaxation of the surrounding medium. The inner reorganization energy upon electron transfer consists of two terms

$$\lambda = \lambda_1(\mathrm{A}) + \lambda_2(\mathrm{D}) \tag{15}$$

$$\lambda_1(\mathrm{A}) = E(\mathrm{A}^-) - E(\mathrm{A}) \tag{16}$$

$$\lambda_2(\mathrm{D}) = E(\mathrm{D}) - E(\mathrm{D}^+) \tag{17}$$

here, $E(\mathrm{A}^-)$ and $E(\mathrm{A})$ are the energies of the neutral acceptor A at the anionic geometry and optimal ground-state geometry, respectively, and $E(\mathrm{D})$ and $E(\mathrm{D}^+)$ are, accordingly, the energies of the radical cation at the neutral geometry and optimal cation geometry. The calculated inner reorganization energy is 0.194 eV, which is similar to the pentacene/C_{60} solar cell (0.1 eV),[3] calculated with DFT. The outer reorganization energy is equal to the change in electronic polarization that arises as a result of the whole (heterojunction and solvent molecule) geometric relaxation, while it is not easy to estimate quantitatively in solid state. The previous experimental result of the smallest reorganization energy of electron transfer in porphyrin−fullerene dyad is 0.23 + 0.11 eV,[38] which is similar to the very small reorganization energy in the photosynthetic reaction center (∼0.2 eV).[39,40] In the case of corrole−fullerene dyads in nonpolar solvent, the overall reorganization energy is 0.5 eV.[11] So, we assume here a value of 0.5 eV for the overall reorganization energy in our calculations.

In the exciton dissociation and charge recombination, $\Delta G = \Delta G_{\mathrm{CT}}$ and ΔG_{CR}, respectively. The ΔG_{CR} can be estimated with

$$\Delta G_{\mathrm{CR}} = E_{\mathrm{IP}}(\mathrm{D}) - E_{\mathrm{EA}}(\mathrm{A}) \tag{18}$$

where $E_{IP}(D)$ and $E_{EA}(A)$ are the ionization potential of the donor and electron affinity of the acceptor, respectively. These quantities are normally estimated from the energies of the highest occupied molecular orbital and lowest unoccupied molecular orbital of the donor and acceptor, respectively.[41] The calculated $\Delta G_{CR} = -1.388$ eV. The ΔG_{CT} can be estimated with the Rehm−Weller equation[42]

$$\Delta G_{CT} = -\Delta G_{CR} - \Delta E_{0-0} - E_b \quad (19)$$

where ΔE_{0-0} is the energy of the lowest excited state of free-base donor and E_b is the exciton binding energy. The calculated ΔG_{CT} is −0.272 eV. The negative ΔG_{CT} means that electron transfer is thermodynamically favorable.

The rates of exciton dissociation and charge recombination can be calculated with

$$k = \sqrt{\frac{4\pi^3}{h^2 \lambda k_B T}} |V_{DA}(S_3) + V_{DA}(S_4)|^2 \exp\left(-\frac{(\Delta G + \lambda)^2}{4\lambda k_B T}\right) \quad (20)$$

The calculated rates of charge transfer and charge recombination are 5.77×10^{11} and 3.76×10^5 s^{-1}, respectively.

4. CONCLUSION

Photoinduced interface exciton−dissociation and charge−recombination in PDDTT−$PC_{60}BM$ heterojunction for an organic solar cell were investigated by means of quantum-chemical calculations, stimulated by the recent experimental reports. It is found that the PDDTT has broad spectral response with low band gap. Also the PDDTT−$PC_{60}BM$ complex has a full range absorption well covering the area from the ultraviolet to near-infrared. The PDDTT−$PC_{60}BM$ heterojunction has small exciton binding energy (0.205 eV), small free-energy change of intermolecular charge transfer and large free-energy change in intermolecular charge recombination, and small reorganization energy (∼0.5 eV). There is strong charge transfer integral (electronic coupling matrix element). Using the Marcus's theory of charge transfer it is predicted that this donor−acceptor heterojunction has fast charge transfer (5.77×10^{11} s^{-1}) and slow charge recombination (3.76×10^5 s^{-1}).

AUTHOR INFORMATION

Corresponding Author

*E-mail: mtsun@aphy.iphy.ac.cn (M. T. Sun).

ACKNOWLEDGMENT

This work was supported by the National Natural Science Foundation of China (Grant Nos. 10874234, 90923003, and 20703064) and the National Basic Research Project of China (Grant Nos. 2009CB930701). M. T. Sun is indebted to the Wenner-Gren Foundation of Sweden for financial support. T. Pullerits acknowledges financial support from the Swedish Research Council and STEM.

REFERENCES

(1) Wohrle, D.; Meissner, D. *Adv. Mater.* **1991**, *3*, 129–138.
(2) Friend, R. H.; Gymer, R. W.; Holmes, A. B.; Burroughes, J. H.; Marks, R. N.; Taliani, C.; Bradley, D. D. C.; Dossantos, D. A.; Bredas, J. L.; Logdlund, M.; Salaneck, W. R. *Nature* **1999**, *397*, 121–127.
(3) Yi, Y.; Coropceanu, V.; Bredas, J. L. *J. Am. Chem. Soc.* **2009**, *131*, 15777–15783.
(4) Sariciftci, N. S.; Smilowitz, L.; Heeger, A. J.; Wudl, F. *Science* **1992**, *258*, 1474–1476.
(5) Guldi, D. M.; Prato, M. *Acc. Chem. Res.* **2000**, *33*, 695–703.
(6) Imahori, H.; Yamada, H.; Guldi, D. M.; Endo, Y.; Shimomura, A.; Kundu, S.; Yamada, K.; Okada, T.; Sakata, Y.; Fukuzumi, S. *Angew. Chem., Int. Ed.* **2002**, *41*, 2344–2347.
(7) Svensson, M.; Zhang, F.; Veenstra, S. C.; Verhees, W. J. H.; Hummelen, J. C.; Kroon, J. M.; Inganas, O.; Andersson, M. R. *Adv. Mater.* **2003**, *15*, 988–991.
(8) Zhang, F.; Perzon, E.; Wang, X.; Mammo, W.; Andersson, M. R.; Inganas, O. *Adv. Funct. Mater.* **2005**, *15*, 745–750.
(9) Gong, X.; Tong, M.; Xia, Y.; Cai, W.; Moon, J.; Cao, Y.; Yu, G.; Shieh, C.; Nilsson, B.; Heeger, A. J. *Science* **2009**, *325*, 1665–1667.
(10) Scharber, M. C.; Muhlbacher, D.; Koppe, M.; Denk, P.; Heeger, A. J.; Waldauf, C.; Brabec, C. *J. Adv. Mater.* **2006**, *18*, 789–794.
(11) D'Souza, F.; Chitta, R.; Ohkubo, K.; Tasior, M.; Subbaiyan, N. K.; Zandler, M. E.; Rogacki, M. K.; Gryko, D. T.; Fukuzumi, S. *J. Am. Chem. Soc.* **2008**, *130*, 14263–14272.
(12) Tong, M.; Sheng, C. X.; Vardeny, Z. V. *Phys. Rev. B* **2007**, *75*, 125207.
(13) Marcus, R. A. *Angew. Chem., Int. Ed. Engl.* **1993**, *32*, 1111–1121.
(14) Veldman, D.; Meskers, S. C. J.; Janssen, R. A. *Adv. Funct. Mater.* **2009**, *19*, 1939–1348.
(15) Sun, M. T.; Kjellberg, P.; Beenken, W. J. D.; Pullerits, T. *Chem. Phys.* **2006**, *327*, 474–484.
(16) Mukamel, S.; Tretiak, S.; Wagersreiter, T.; Chernyak, V. *Science* **1997**, *277*, 781–787.
(17) Frisch, M. J.; Trucks, G. W.; Schlegel, H. B.; Scuseria, G. E.; Robb, M. A.; Cheeseman, J. R.; Scalmani, G.; Barone, V.; Mennucci, B.; Petersson, G. A.; et al. *Gaussian 09, Revision A.02*; Gaussian, Inc.: Wallingford, CT, 2009.
(18) Hohenberg, P.; Kohn, W. *Phys. Rev.* **1964**, *136*, B864–B687.
(19) Becke, A. D. *Phys. Rev. A* **1988**, *38*, 3098–3100.
(20) Tolbert, L. M. *Acc. Chem. Res.* **1992**, *25*, 561–568.
(21) O'Boyle, N. *GaussSum, Revision 2.1*, http://GaussSum.sf.net.
(22) Gross, E. K. U.; Kohn, W. *Phys. Rev. Lett.* **1985**, *55*, 2850–2582.
(23) Yanai, T.; Tew, D.; Handy, N. *Chem. Phys. Lett.* **2004**, *393*, 51–57.
(24) Tretiak, S.; Igumenshchev, K.; Chernyak, V. *Phys. Rev. B* **2005**, *71*, 033201.
(25) Voityuk, A. A. *J. Chem. Phys.* **2006**, *124*, 064505.
(26) Kjellberg, P.; He, Z.; Pullerits, T. *J. Phys. Chem. B* **2003**, *107*, 13737–13742.
(27) Jespersen, K. G.; Beenken, W. J. D.; Zausjitsyn, Y.; Yartsev, A.; Andersson, M.; Pullerits, T.; Sundström, V. *J. Chem. Phys.* **2004**, *121*, 12613–12617.
(28) Beenken, W. J. D.; Pullerits, T. *J. Phys. Chem. B* **2004**, *108*, 6164–6169.
(29) Zojer, E.; Buchacher, P.; Wudl, F.; Cornil, J.; Ph. Calbert, J.; Bredas, J. L.; Leising, G. *J. Chem. Phys.* **2000**, *113*, 10002. Rissler, J.; Bassler, H.; Gebhard, F.; Schwerdtfeger, P. *Phys. Rev. B* **2001**, *64*, 045122.
(30) Barford, W.; Trembath, D. *Phys. Rev. B* **2009**, *80*, 165418.
(31) Collini, E.; Scholes, G, D. *Science* **2001**, *323*, 369–373.
(32) Grage, M. M. L.; Pullerits, T.; Ruseckas, A.; Theander, M.; Inganäs, O; Sundström, V. *Chem. Phys. Lett.* **2001**, *339*, 96–102.
(33) Grage, M. M. L.; Zaushitsyn, Y.; Yartsev, A.; Chachisvilis, M.; Sundström, V.; Pullerits, T. *Phys. Rev. B* **2003**, *67*, 205207.
(34) Emelianova, E. V.; van der Auweraer, M.; Bassler, H. *J. Chem. Phys.* **2008**, *128*, 224709.
(35) Zhen, C. G.; Becker, U.; Kieffer, J. *J. Phys. Chem. A* **2009**, *113*, 9707–9714.
(36) Scholes, G. D.; Rumbles, G *Nat. Mater.* **2006**, *5*, 683–696.
(37) Bredas, J. L.; Beljonne, D.; Coropceanu, V.; Cornil, J. *Chem. Rev.* **2004**, *104*, 4971–5003.
(38) Imahori, H.; Tkachenko, N. V.; Vehmanen, V.; Tamaki, K.; Lemmetyinen, H.; Sakata, Y.; Fukuzumi, S. *J. Phys. Chem. A* **2001**, *105*, 1750–1756.

(39) Moser, C. C.; Keske, J. M.; Warncke, K.; Farid, R. S.; Dutton, P. L. *Nature* **1992**, *355*, 796–802.
(40) Marcus, R. A.; Sutin, N. *Biochim. Biophys. Acta* **1985**, *811*, 265–322.
(41) Zhang, X.; Chi, L.; Ji, S.; Wu, Y.; Song, P.; Han, K.; Guo, H.; James, T. D.; Zhao, J. *J. Am. Chem. Soc.* **2009**, *131*, 17452–17463.
(42) Kavarnos, G.; Turro, N. J. *Chem. Rev.* **1986**, *86*, 401–449.